Supporting Information for

Significant source of secondary aerosol: formation from gasoline

evaporation emissions in the presence of SO_2 and NH_3

Tianzeng Chen[1, 3, a], Yongchun Liu[2, a], Qingxin Ma[1, 3, 4, *], Biwu Chu[1, 3, 4], Peng Zhang [1],

Changgeng Liu[1], Jun Liu[1, 3], Hong He[1, 3, 4, *]

[1] State Key Joint Laboratory of Environment Simulation and Pollution Control, Research Center for

Eco-Environmental Sciences, Chinese Academy of Sciences, Beijing 100085, China

[2] Beijing Advanced Innovation center for Soft Matter Science and Engineering, Beijing University

of Chemical Technology, Beijing 100029, China

[3] University of Chinese Academy of Sciences, Beijing 100049, China

[4] Center for Excellence in Regional Atmospheric Environment, Institute of Urban Environment,

Chinese Academy of Sciences, Xiamen 361021, China

[a] These authors contributed equally to this work and should be considered as co-first authors

Corresponding authors: qxma@rcees.ac.cn (Qingxin Ma), and honghe@rcees.ac.cn (Hong He)

S1. Vapor wall loss and gas-particle partitioning timescales

The loss of vapor by condensation onto the wall is generally considered to be a first-order process, which can be characterized by the first-order wall-loss coefficient k_w (s^{-1}). According to the following equation reported by McMurry and Grosjean (1985), the value of k_w is equal to:

$$k_w = \frac{A}{V} \times \frac{\alpha_w \bar{c}}{1.0 + \frac{\pi}{2} \times \left[\frac{\alpha_w \bar{c}}{4(k_e D_{gas})^{0.5}}\right]}$$

in which A and V are the surface and volume of the smog chamber, respectively. For our cuboid smog chamber ($L \times W \times H = 3.0 \times 2.5 \times 4.0$ m), A=59 m^2, V=30 m^3. α_w is the mass accommodation coefficient of vapors onto the chamber walls, $\bar{c}$ is the mean thermal speed of the molecules, k_e is the coefficient of eddy diffusion, and D_{gas} is the gas-phase diffusivity.

For a given vapor molecule, the mean thermal speed $\bar{c}$ could be calculated according to the following equation:

$$\bar{c} = \sqrt{\frac{8RT}{\pi MW}}$$

in which R is the ideal gas constant (i.e., 8.314 J mol^{-1} K^{-1}), T is the experimental temperature (T=299.15 K in this study), and MW is the molecular weight (an upper bound and a lower bound of molecular mass of organic vapors was adopted, i.e., 100 g mol^{-1} and 300 g mol^{-1} in this study).

D_{gas} is assumed to vary with molecular weight (MW) and is equal to $D_{CO_2}(MW_{CO_2}/MW)$, with $D_{CO_2} = 1.38 \times 10^{-5}$ m^2 s^{-1}. Therefore, this leaves k_e and α_w as the two key unknowns. For the value of k_e, 0.015 s^{-1} was estimated according to the values reported by previous studies for a 28 m^3 Caltech chamber (Loza et al., 2012; McMurry and Rader, 1985; Zhang et al., 2014). For the value of α_w, 10^{-5} was adopted according to the experimental results of Matsunaga and Ziemann (2010).

35   Then the timescale associated with vapor-wall loss ($\tau_{\text{g-w}}$) is calculated to be:

36    $$\tau_{g-w} = k_w^{-1}$$

37   for the timescale associated with reaching gas-to-particle partitioning equilibrium ($\overline{\tau}_{\text{g-p}}$), which

38   varies with particle number concentration and diameter, and could be approximately calculated to be:

39    $$\overline{\tau}_{g-p} = (2\pi N_p \overline{D_p} D_{gas} \overline{F_{FS}})^{-1}$$

40   in which N_p is the particle number concentration, $\overline{D_p}$ is the particle mean diameter, D_{gas} is the gas-

41   phase diffusivity and $\overline{F_{FS}}$ is the correction to the mass transfer flux due to noncontinuum effects and

42   imperfect accommodation given in the following equation:

43    $$\overline{F_{FS}} = \frac{0.75\alpha(1 + k_n)}{k_n^2 + k_n + 0.283 k_n \alpha + 0.75\alpha}$$

44   in which α is the mass accommodation coefficient onto particles, for which the value of 0.002 was

45   adopted in this study, and k_n is the Knudsen number, defined as:

46    $$k_n = \lambda / R_p$$

47   in which λ is the gas mean free path, which could be calculated as following equation:

48    $$\lambda = \frac{3 D_{gas}}{\overline{c}}$$

49   In our study, the SA yields were underestimated by a factor of 1.97−2.82 fold when considering

50   the ratio of these two timescales (i.e., $\overline{\tau}_{\text{g-p}}/\tau_{\text{g-w}}$), which showed a decreasing trend with increasing SO_2

51   and NH_3 initial concentrations, suggesting that an increasing proportion of vapors is partitioned onto

52   the suspended particle surface rather than the chamber wall. Meanwhile, the wall loss of sulfuric acid

53   gas was also considered using this ratio (i.e., $\overline{\tau}_{\text{g-p}}/\tau_{\text{g-w}}$) to correct the sink of sulfur species.

S2. Positive matrix factorization (PMF)

55   Positive Matrix Factorization (PMF) (Paatero, 1997; Paatero and Tapper, 1994) is a receptor model

56   and multivariate factor analysis tool that decomposes a matrix of speciated sample data into two matrices,

57   namely factor contributions and factor profiles. In recent years, the PMF model was used for the analysis

58   of high-resolution (HR) mass spectra data which can provide better separation of different organic

59   components (Liu et al., 2014). This model was expressed as a bilinear factor model, namely, $x_{ij} = \sum_p g_{ip} f_{pj}$

60    $+ e_{ij}$, where i and j refer to values of j species in i samples, respectively, p is the number of factors in the

61   solution, and used a least-squares fitting process, minimizing a quality of fit parameter. In our study, we

62   used the PMF software together with a modified version of the CU AMS PMF Execute Calcs Tool v

63   2.06, which was developed by Ulbrich et al. (2009), to analyze the HR mass spectra (*m/z* 12 − 170)

64   (Zhang et al., 2011). The data and noise matrices input into the PMF analysis were generated from the

65   PIKA version 1.15D. Ions were classified and down-weighted according to the signal-to-noise ratios

66   (SNR). 0.2<SNR<2 was classified as the weak ions and down-weighted by a factor of 2, SNR<0.2 was

67   bad ions and removed from the analysis and noise values of CO_2^+-related peaks at m/z 16 (O), 17 (HO),

68   18 (H_2O), 28 (CO), and 44 (CO_2) were down-weighted.

    Table S1. The volume fraction of detected compounds for gasoline utilized in this study.

Compounds	Volume Fraction (v/v %)	Compounds	Volume Fraction (v/v %)
1,3-Butadiene	10.67	n-Octane	1.71
1-Pentene	0.00	p-Xylene and m-Xylene	2.28
trans-2-Pentene	0.06	Ethylbenzene	1.82
cis-2-Pentene	0.06	Nonane	0.75
Isoprene	1.33	o-Xylene	1.09
2,2-Dimethylbutane	1.11	Styrene	0.00
2,3-Dimethylbutane	7.74	Isopropylbenzene	0.30
2-Methylpentane	7.83	n-Propylbenzene	2.11
3-Methylpentane	5.63	1,3,5-Trimethylbenzene	0.93
1-Hexene	0.00	m-Ethyltoluene	0.93
n-Hexane	9.89	p-Ethyltoluene	0.93
2,4-Dimethylpentane	2.42	n-Decane	0.00
Methylcyclopentane	3.70	o-Ethyltoluene	0.60
Cyclohexane	1.91	1,2,4-Trimethylbenzene	5.12
2-Methylhexane	2.18	1,2,3-Trimethylbenzene	0.92
3-Methylhexane	2.62	m-Diethylbenzene	0.17
2,3-Dimethylpentane	2.53	p-Diethylbenzene	0.17
Benzene	0.58	n-Undecane	0.00
2,2,4-Trimethylpentane	3.87	n-Dodecane	0.83
n-Heptane	5.12		
Methylcyclohexane	2.43		
2,3,4-Trimethylpentane	1.20		
2-Methylheptane	0.62		
3-Methylheptane	0.59		
Toluene	4.90		
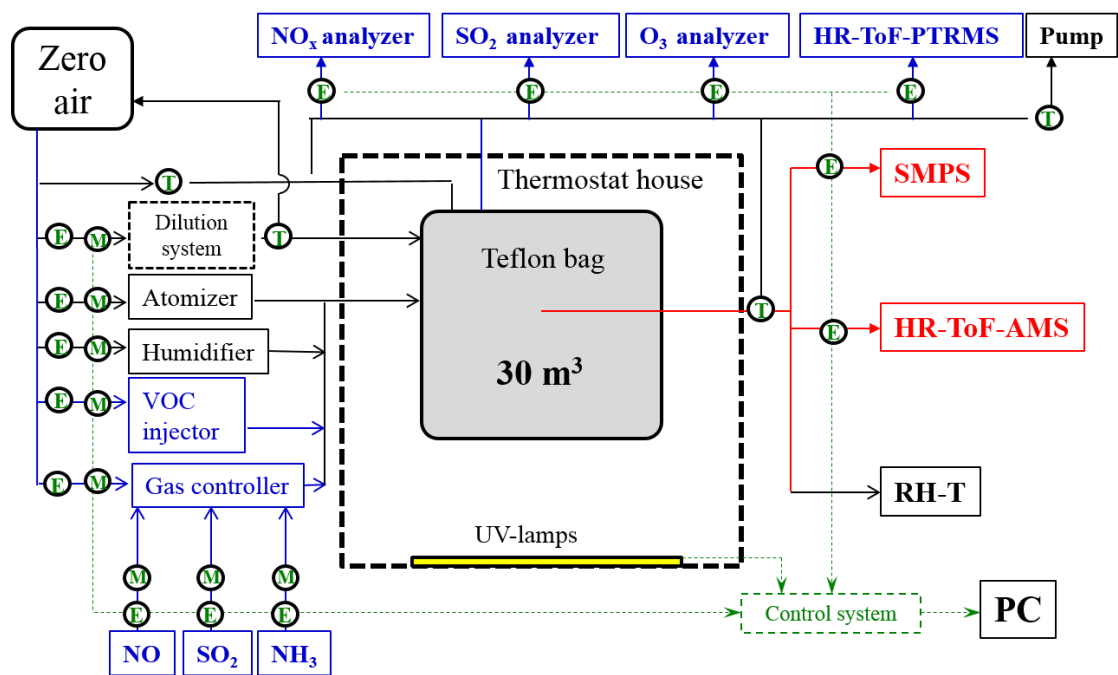
71

72   Fig. S1. Schematic of the RCEES-CAS smog chamber facility. E: Electromagnetic valve; T: Three-way valve. M:

73   Mass flow controller.
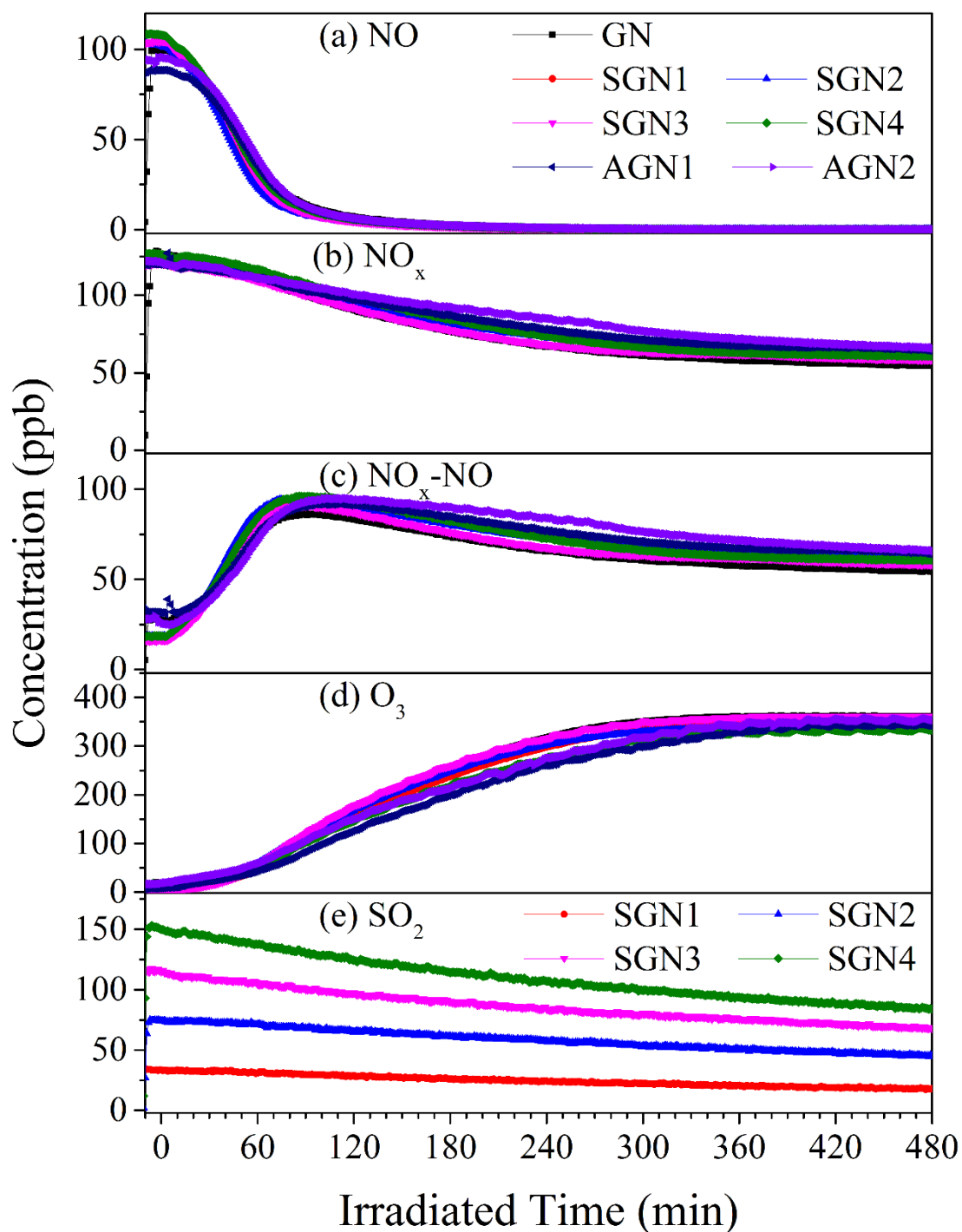
Fig. S2. Time variations of inorganic gas-phase species (a) NO, (b) NO_x, (c) NO_x-NO, (d) O_3, and (e) SO_2 in photo-oxidation of gasoline/NO_x in the presence or absence of SO_2 and NH_3. Letters in abbreviations represent the reactants introduced into the chamber reactor, i.e., "G" represents gasoline, "N" represents nitrogen oxides, "S" represents sulfur dioxide, "A" represents ammonia.
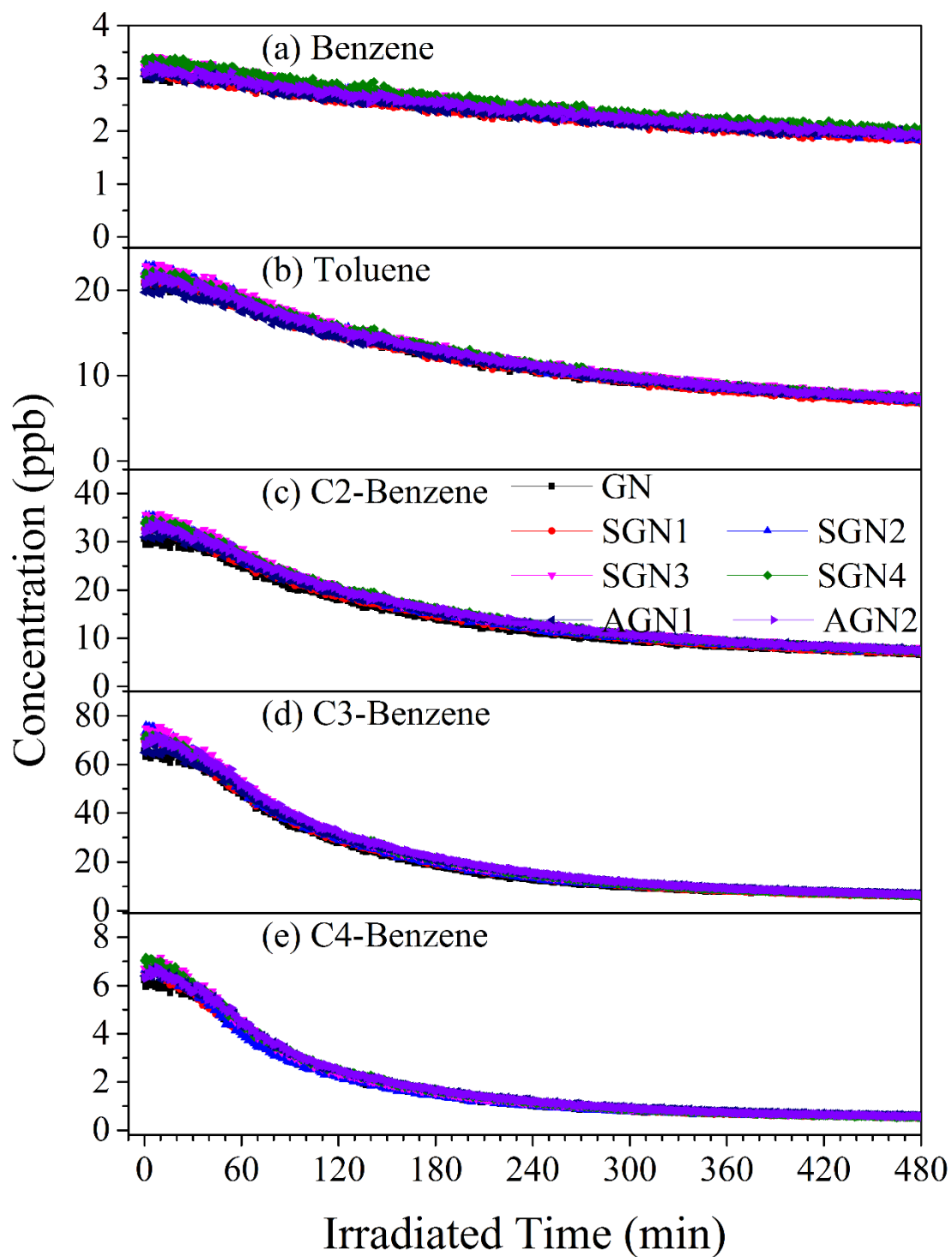
Fig. S3. Time variations of organic gas-phase species (a) Benzene, (b) Toluene, (c) C2-Benzene, (d) C3-Benzene, and (e) C4-Benzene in photo-oxidation of gasoline/NO_x in the presence or absence of SO_2 and NH_3. Letters in abbreviations represent the reactants introduced into the chamber reactor, i.e., "G" represents gasoline, "N" represents nitrogen oxides, "S" represents sulfur dioxide, "A" represents ammonia.
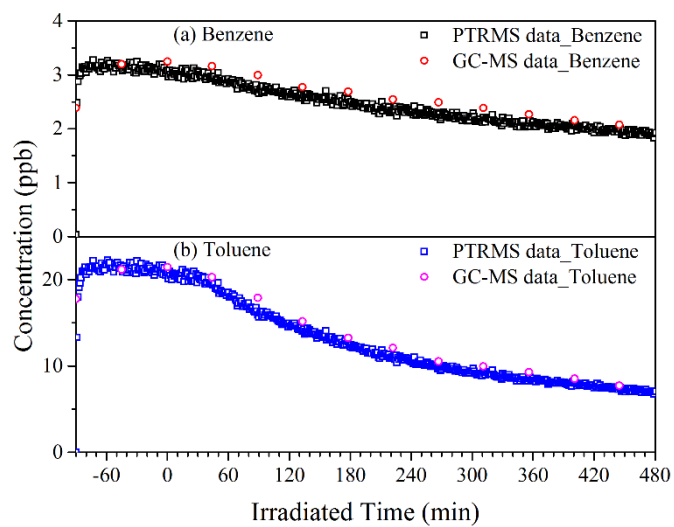
84

85   Fig. S4. Time variations of (a) Benzene and (b) Toluene measured by HR-ToF-PTRMS and GC-MS during a typical chamber

86   experiment (experiment GN).
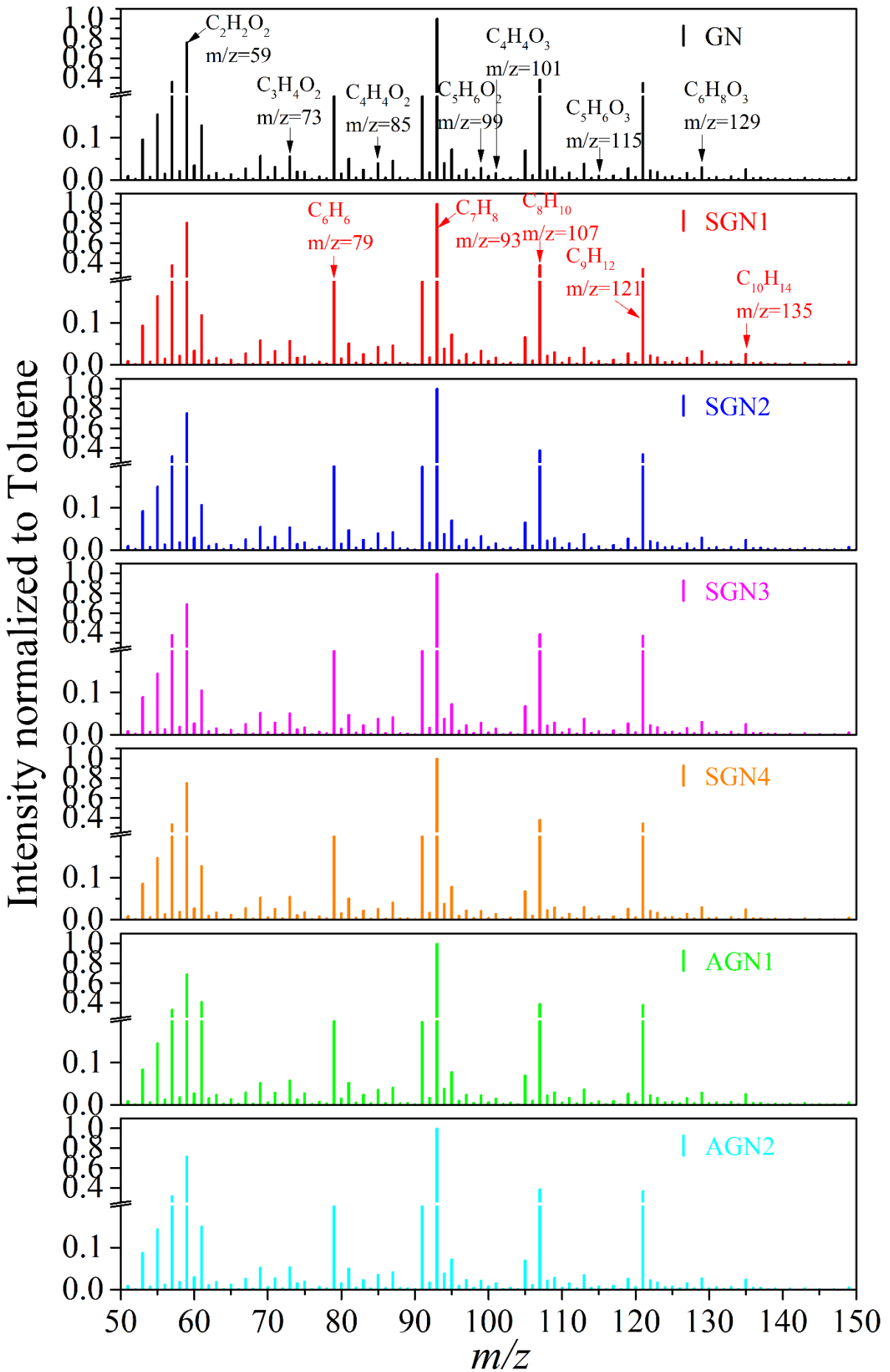
88   Fig. S5. Comparison of the mass spectrum of gas-phase species measured by HR-ToF-PTRMS after 480 min of the photo-

89   oxidation reaction at different concentrations of SO_2 or NH_3. Each bar is represented as an intensity normalized to m/z 93 (i.e.,

90   protonated toluene, $C_7H_9^+$), which had the most abundant intensity in the gasoline vapor. The mass peaks at m/z 59, 73, 85, 99,

91   101, 115, and 129 were tentatively assigned to the protonated ions of $C_2H_2O_2$ (glyoxal), $C_3H_4O_2$ (methylglyoxal), $C_4H_4O_2$

92   (butenedial), $C_5H_6O_2$ (4-oxo-2-pentenal), $C_4H_4O_3$ (2,3-epoxybutandial), $C_5H_6O_3$ (2-methyl-2,3-epoxybutandial), and $C_6H_8O_3$

93   (2,3-epoxy-1,4-dicarbonyl), respectively. And m/z 79, 93, 107, 121, and 135 were assigned to the protonated ions of benzene,

94   toluene, C2-benzene, C3-benzene, and C4-benzene, respectively.
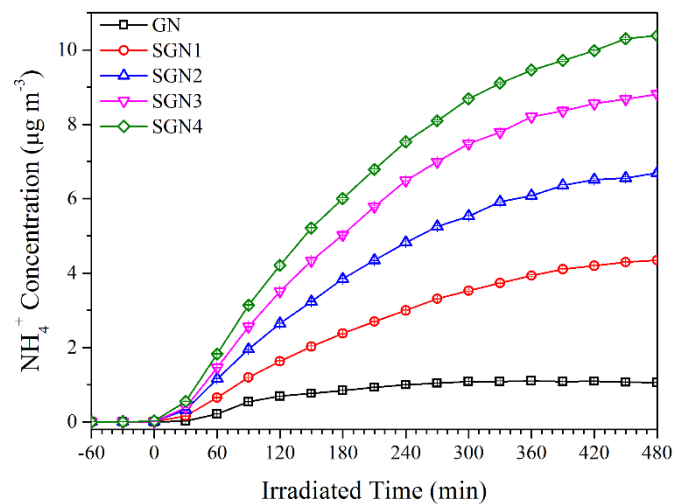
95

96   Fig. S6. Time series of the ammonium aerosol formed during the photo-oxidation experiments with different SO_2

97   concentrations without adding additional gaseous NH_3 (i.e., GN, SGN1, SGN2, SGN3 and SGN4 listed in Table S2).

98
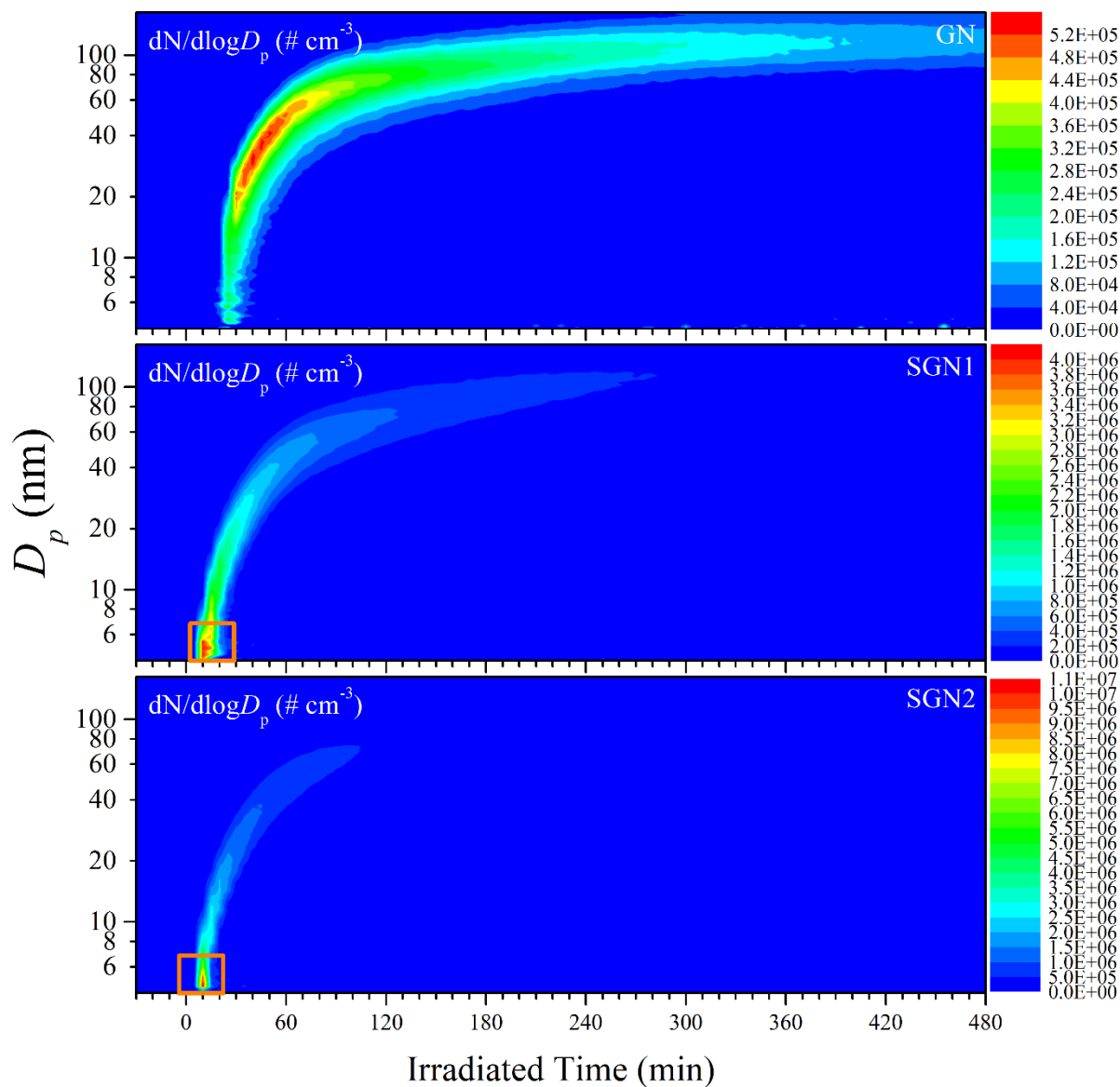
Fig. S7. Time series of the smaller size distributions (4−160 nm) derived from SMPS equipped with a nanometer differential

mobility analyzer (Nano-DMA) for the generated secondary aerosol during the photo-oxidation experiments with different

SO_2 concentrations.
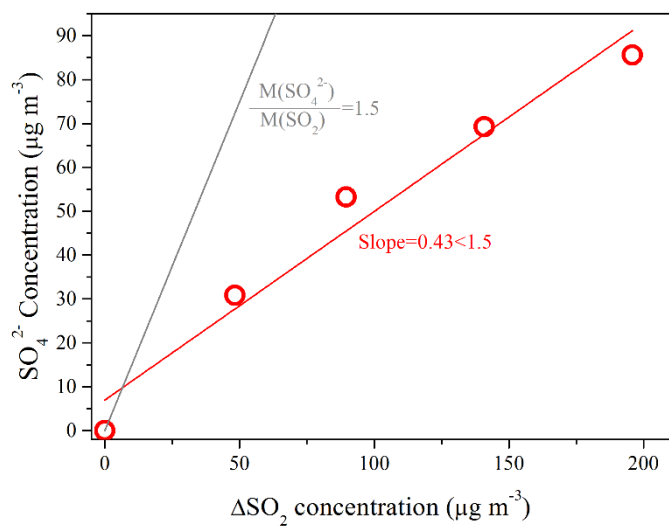
102

103   Fig. S8. Amounts of consumed SO_2 as a function of formed SO_4^{2-} under different SO_2 initial concentrations conditions. The

104   red line is a linear fitting of all the corresponding data points. $M(SO_4^{2-})$ and $M(SO_2)$ represent the molecular weight of SO_4^{2-}

105   and SO_2, respectively, and the ratio of them is 1.5.
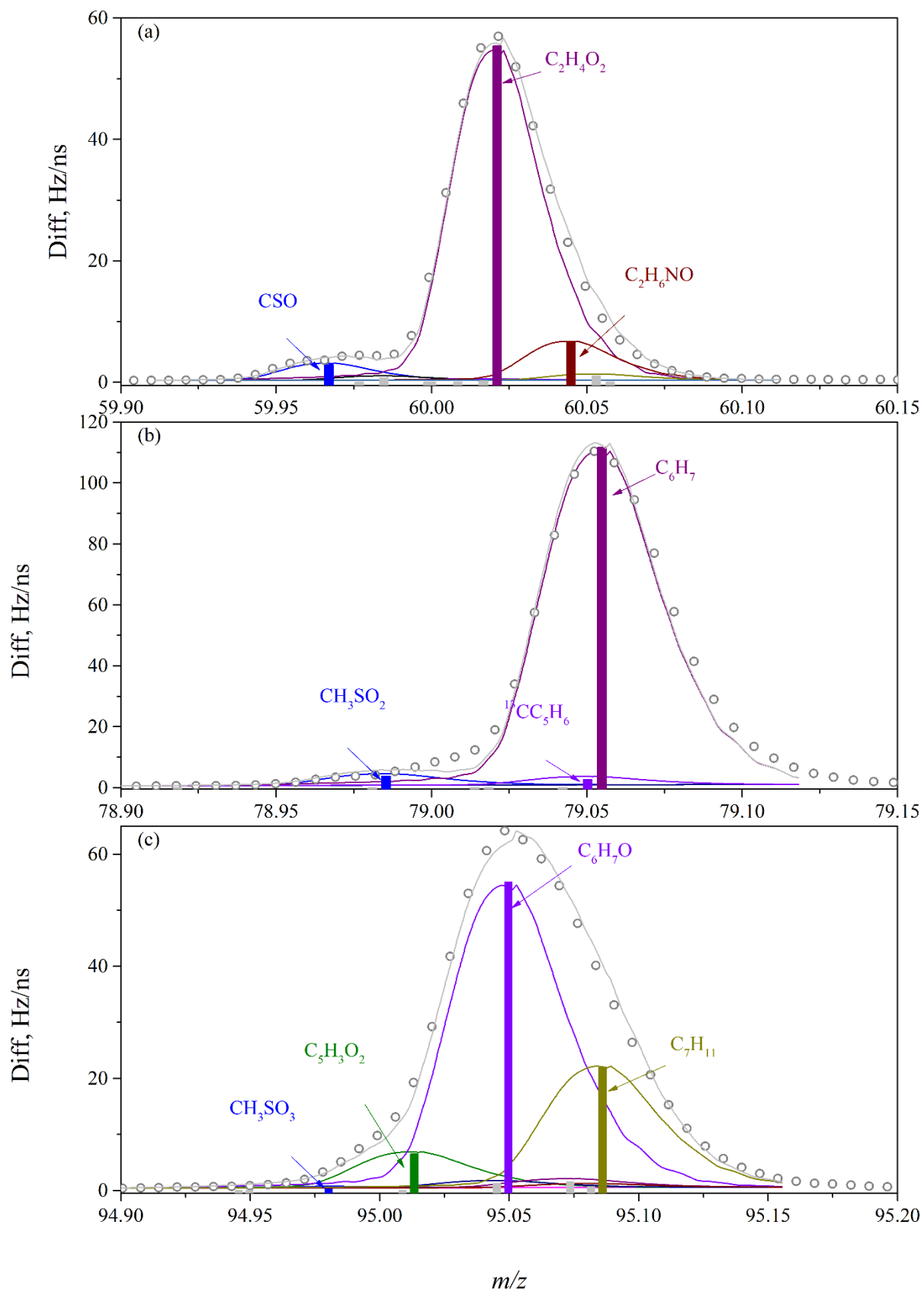
106

107 Fig. S9. Fitted peaks of average W-mode mass spectrum of organosulfur compounds (OS), (a) CSO^+, (b) $CH_3SO_2^+$, (c)

108 $CH_3SO_3^+$.
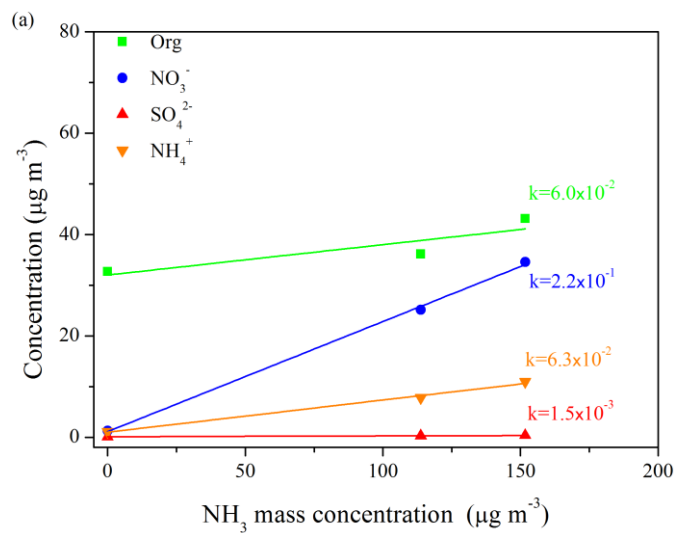
109
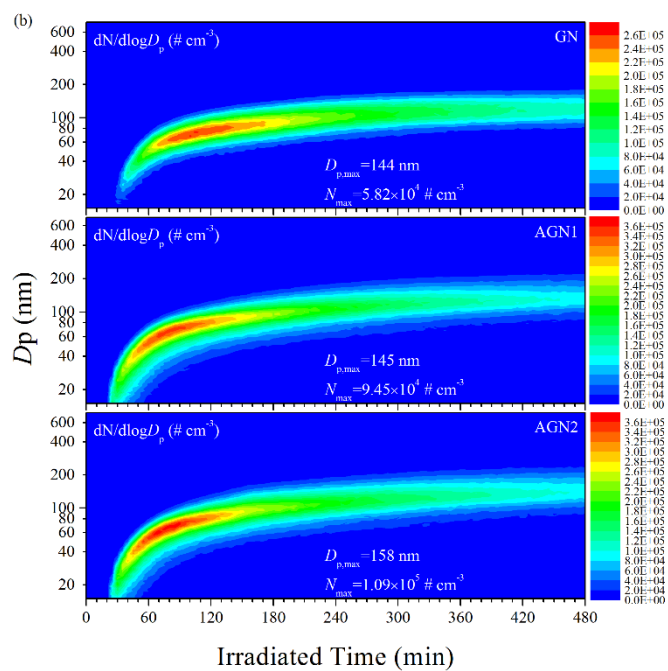
110
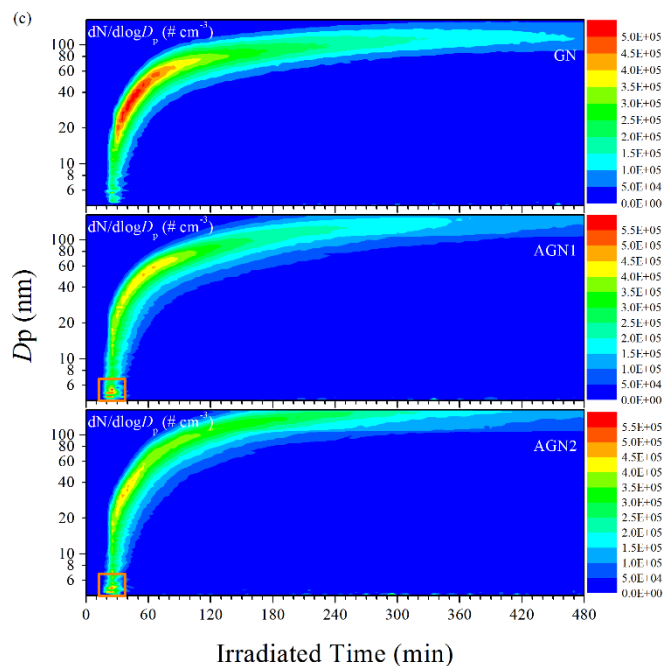
111

112   Fig. S10. (a) Linear relationship between the concentration of chemical species and NH$_3$ under different NH$_3$ initial

113   concentration conditions. Each line (green (organic), blue (nitrate), red (sulfate), and orange (ammonium)) represents a linear

114   fitting and the k values are the corresponding slopes for each chemical species. (b) Time series of the size distributions (20−700

115   nm) for the secondary aerosol generated during the photo-oxidation experiments with different NH$_3$ concentrations. $D_{p,max}$ and

116   N_{max} represent the maximal diameter and number concentration of generated secondary aerosol, respectively, during each

117   photo-oxidation experiment. (c) Time series of the smaller size distributions (4−160 nm) derived from SMPS equipped with a

118   nanometer differential mobility analyzer (Nano-DMA) for the generated secondary aerosol during the photo-oxidation

119   experiments with different NH$_3$ concentrations.
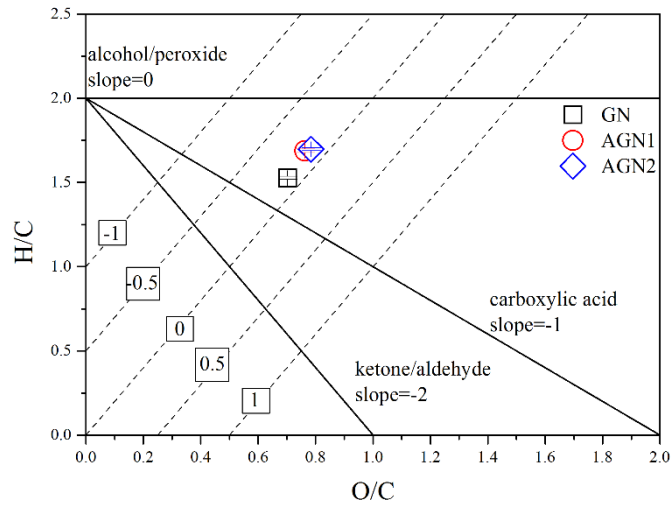
120

121   Fig. S11. Average O/C and H/C in SOA formed from the photo-oxidation of gasoline vapor at different concentrations of NH_3

122   (Exps. GN, AGN1 and AGN2).
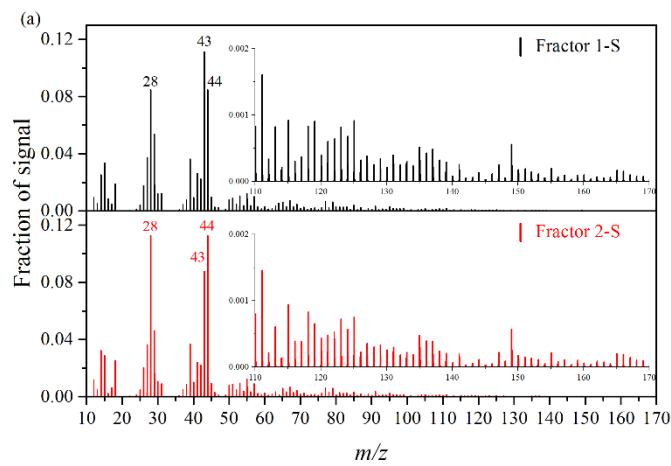
123
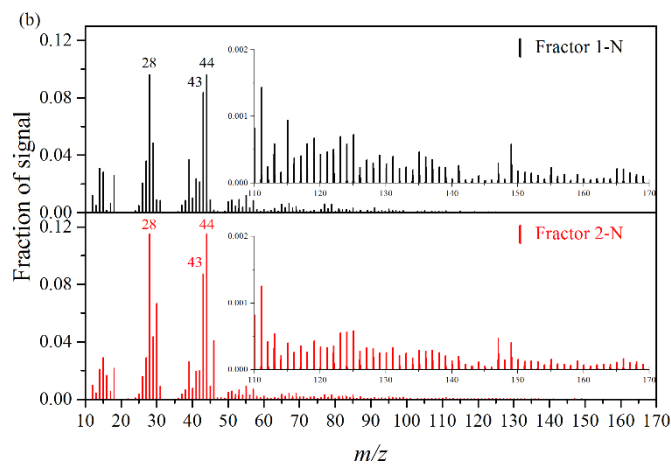
124

125   Fig. S12. Mass spectra of the two factors identified from the PMF analysis to the AMS data derived from the experiments at

126   different concentrations of (a) SO_2 (Exp. GN, SGN1, SGN2, SGN3 and SGN4) and (b) NH_3 (Exp. GN, AGN1 and AGN2).
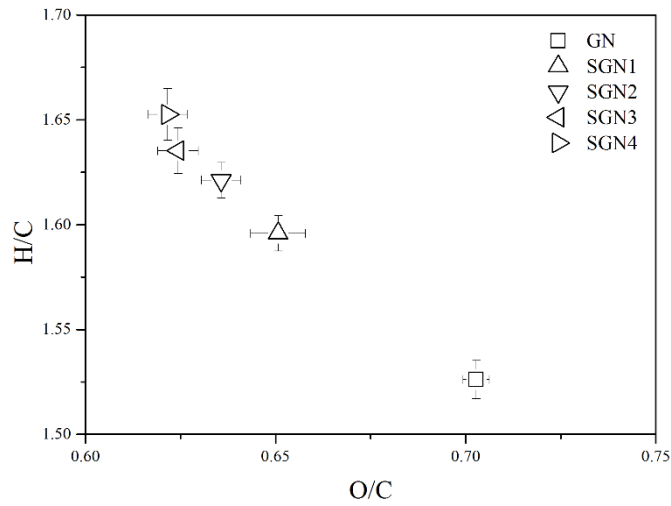
127

128   Fig. S13. Average O/C and H/C in SOA formed from the photo-oxidation of gasoline vapor at different concentrations of SO_2

129   (Exp. GN, SGN1, SGN2, SGN3 and SGN4).
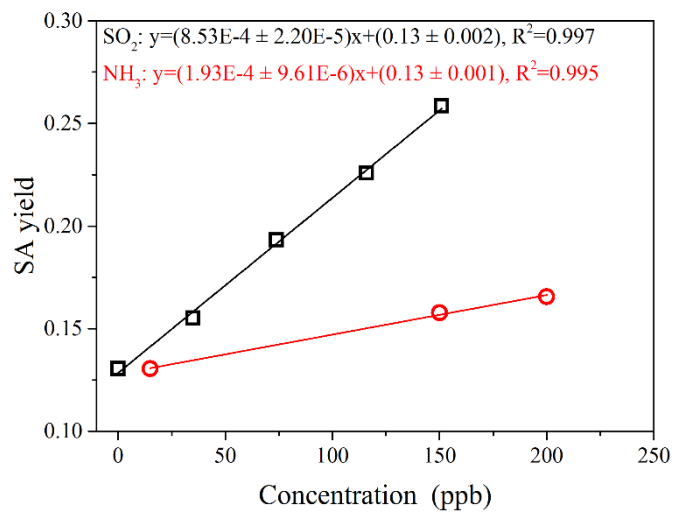
130

131   Fig. S14. Linear relationship between the concentration of SO_2 (or NH_3) and the SA yield.

132 **References**

133   Liu, Y., Li, S. M., and Liggio, J.: Technical Note: application of positive matrix factor analysis in

134   heterogeneous kinetics studies utilizing the mixed-phase relative rates technique, Atmos. Chem. Phys.,

135   14, 9201-9211, doi: 10.5194/acp-14-9201-2014, 2014.

136   Loza, C. L., Chhabra, P. S., Yee, L. D., Craven, J. S., Flagan, R. C., and Seinfeld, J. H.: Chemical

137   aging of m-xylene secondary organic aerosol: laboratory chamber study, Atmos. Chem. Phys., 12, 151-

138   167, doi: 10.5194/acp-12-151-2012, 2012.

139   Matsunaga, A., and Ziemann, P. J.: Gas-wall partitioning of organic compounds in a teflon film

140   chamber and potential effects on reaction product and aerosol yield measurements, Aerosol Sci. Tech.,

141   44, 881-892, doi: 10.1080/02786826.2010.501044, 2010.

142   McMurry, P. H., and Grosjean, D.: Gas and aerosol wall losses in Teflon film smog chambers,

143   Environ. Sci. Technol., 19, 1176-1182, doi: 10.1021/es00142a006, 1985.

144   McMurry, P. H., and Rader, D. J.: Aerosol wall losses in electrically charged chambers, Aerosol Sci.

145   Tech., 4, 249-268, doi: 10.1080/02786828508959054, 1985.

146   Paatero, P., and Tapper, U.: Positive matrix factorization: a non-negative factor model with optimal

147   utilization of error estimates of data values, Environmetrics, 5, 111-126, doi: 10.1002/env.3170050203,

148   1994.

149   Paatero, P.: Least squares formulation of robust non-negative factor analysis, Chemom. Intell. Lab.

150   Syst., 37, 23-35, doi: 10.1016/S0169-7439(96)00044-5, 1997.

151   Ulbrich, I. M., Canagaratna, M. R., Zhang, Q., Worsnop, D. R., and Jimenez, J. L.: Interpretation

152   of organic components from positive matrix factorization of aerosol mass spectrometric data, Atmos.

153   Chem. Phys., 9, 2891-2918, doi: 10.5194/acp-9-2891-2009, 2009.

154   Zhang, Q., Jimenez, J. L., Canagaratna, M. R., Ulbrich, I. M., Ng, N. L., Worsnop, D. R., and Sun,

155   Y.: Understanding atmospheric organic aerosols via factor analysis of aerosol mass spectrometry: a

156   review, Anal. Bioanal. Chem., 401, 3045-3067, doi: 10.1007/s00216-011-5355-y, 2011.

157   Zhang, X., Cappa, C. D., Jathar, S. H., McVay, R. C., Ensberg, J. J., Kleeman, M. J., and Seinfeld,

158   J. H.: Influence of vapor wall loss in laboratory chambers on yields of secondary organic aerosol, Proc.

159   Natl. Acad. Sci. USA, 111, 5802-5807, doi: 10.1073/pnas.1404727111, 2014.